

Cross-well imaging by the CDP stacking and the diffraction stacking with velocity analysis

Jun MATSUSHIMA*, Shuichi ROKUGAWA**
Toshiyuki YOKOTA*³ and Teruki MIYAZAKI*³

ABSTRACT

This paper describes two types of data processing applied to primary reflections and diffractions observed in a cross-well seismic survey. These are the CDP (Common Depth Point) stacking and the diffraction stacking with velocity analysis. The conventional processing of surface seismic reflection method is modified and applied to cross-well reflection and diffraction data. One of the biggest advantages of these methods is that data processing can be performed without information from velocity tomograms. So, imaging can be achieved even in the lower part of a well beyond the coverage of cross-well travel time tomography.

Firstly, the data processing methods are presented. Numerical simulation models are used for evaluation of these data processing methods. Secondly, the effectiveness and robustness of these methods for noisy or complicated data are shown. Thirdly, preliminary examples of the application of these methods to field data in a geothermal area are presented. Adequate stacked records could not be obtained by application of the CDP stacking and improved stacked records were produced by using the proposed diffraction stacking. The reasons for this result are discussed.

An important characteristic of the proposed data processing methodology is insensitive to velocity field. In this respect, it has potential application for rough imaging, as a first step before more precise imaging is undertaken, especially in geothermal or other inhomogeneous areas.

Key words: cross-well, velocity analysis, CDP stacking, diffraction stacking

1. INTRODUCTION

Cross-well seismic methods have the potential to achieve a higher resolution imaging than surface seismic methods for targets between

wells. Direct-arrival traveltimes tomography is the most popular method and it gives a velocity distribution between wells. However, the observed data in a cross-well geometry have enough information to achieve higher resolution than that

1996年2月19日原稿受付；1996年11月13日受理
物理探査学会第92, 93回（平成7年度）学術講演会にて一部発表

* 地質調査所（現 東京大学工学部）
〒305 茨城県つくば市東1-1-3
（〒113 東京都文京区弥生2-11-16）

** 東京大学大学院工学系研究科
〒113 東京都文京区本郷7-3-1

*³ 地質調査所
〒305 茨城県つくば市東1-1-3

Manuscript received February 19, 1996; Accepted November 13, 1996.

A part of this paper was presented at the 92nd and 93rd SEGJ Conference, 1995.

* Geological Survey of Japan (Presently Faculty of Engineering, The University of Tokyo)
1-1-3, Higashi, Tsukuba, Ibaraki 305, Japan
(2-11-16, Yayoi, Bunkyo-ku, Tokyo 113, Japan)

** Division of Engineering, Graduate School, The University of Tokyo 7-3-1, Hongo, Bunkyo-ku, Tokyo 113, Japan

*³ Geological Survey of Japan
1-1-3, Higashi, Tsukuba, Ibaraki 305, Japan

produced by direct-arrival traveltimes tomography. Some authors have demonstrated cross-well reflector imaging as one technique which can produce higher resolution subsurface imaging (HARRIS *et al.*, 1992, LAZARATOS *et al.*, 1993, SAM *et al.*, 1992, VAN SHAACK *et al.*, 1992). They have produced depth-migrated images by combining wavefield separation processing and migration processing, using the velocity information obtained from direct-arrival traveltimes tomography.

In a volcanic or highly fractured area (generally in inhomogeneous media), cross-well records with a signal to noise ratio high enough for the use of seismic reflected or scattered wavefields are rarely acquired, because of unsatisfactory observation system or the inhomogeneity. Generally, for the use of seismic reflected or scattered wavefields in a cross-well geometry, those wavefields must be extracted from observed cross-well seismic data. But it is not easy to detect and extract reflections or diffractions clearly from observed data only by using wavefield separation techniques. Problems are caused by the source/receiver geometrical arrangements, the contamination of tubewaves, the inhomogeneity of the media and other factors. It is indispensable for this method both to improve the signal to noise ratio of data and to develop a robust data processing methodology.

Velocity analysis (the main element of surface seismic data processing) can be a useful tool for detecting a pattern of reflected or scattered wavefields. It may be regarded as a kind of matching against characteristic patterns (e.g. the hyperbola pattern caused by reflection events in a CDP ensemble). In this paper, velocity analysis is modified and applied to a cross-well seismic geometry and further for detecting a pattern caused

by diffraction events. Stacked records can be obtained based on results of velocity analysis. The advantages of these methods are that data processing can be performed without using the information from velocity tomograms and that imaging can be achieved even in the lower part of a well beyond the coverage of cross-well travel time tomography. The methods are also insensitive to velocity field. The disadvantage of these methods is that complicated structures cannot be imaged precisely because of insensitivity to velocity field. They may be used to obtain rough imaging as the first step, in order to take the next step and perform more precise imaging, especially in geothermal or other inhomogeneous areas.

2. DATA PROCESSING

2.1 VELOCITY ANALYSIS AND CDP STACKING USING REFLECTIONS

This type of data processing was described in detail in ROKUGAWA and MATSUSHIMA, 1995. This section gives only an outline of the methodology.

The following equation is the travel time equation of reflection for a cross-well geometry, assuming horizontal layering and straight raypaths;

$$t = \sqrt{\left(2T(0) - \frac{X_s + X_r}{V}\right)^2 + \left(\frac{L}{V}\right)^2} \quad (1)$$

$$\left(T(0) = \frac{Z}{V}\right)$$

where $T(0)$ is one way normal travel time, V is velocity and the other parameters are as shown in Figure 1(a).

The typical procedure of this method is as follows;

step 1: Set a CDP location and the standard

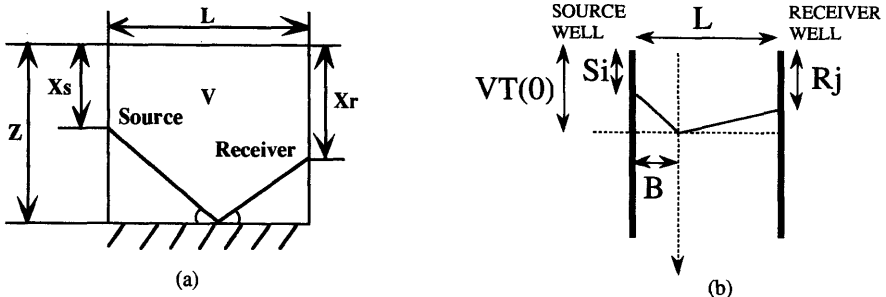


Fig. 1 Parameters for calculus of travel time in case of (a) the CDP stacking and (b) the diffraction stacking.

depth (time=0) for the one way normal time $T(0)$.

step 2 : Assume a pair of values for V and $T(0)$ in equation (1)

step 3 : Obtain the depth by the product of V and $T(0)$.

step 4 : Select pairs of source and receiver which compose the common reflection point gather.

step 5 : Substitute X_s and X_r into equation (1) and obtain the travel time of reflection for each pair. Here, X_s and X_r are the positions of each pair of source and receiver obtained from step 4.

step 6 : Add the amplitude corresponding to the travel time obtained from step 5 and divide the added amplitude by the stack number. This value gives the concentration of the reflection energy.

step 7 : Repeat steps 2 to 6.

This procedure gives a velocity analysis panel at the CDP location. This panel is a table of numbers as a function of velocity versus one-way normal time. Velocity-time pairs are selected from this panel based on maximum coherency peaks. A series of values along these velocity-time pairs makes a CDP stacked trace.

2.2 VELOCITY ANALYSIS AND DIFFRACTION STACKING USING DIFFRACTIONS

Velocity analysis using diffractions is similar to velocity analysis using reflections. Figure 2 illustrates the comparison of stacked waves between common reflection point and common diffraction point. In the case of velocity analysis using reflections, only common reflected waves are stacked at a point (Figure 2(a)). On the other hand, in the case of velocity analysis using diffrac-

tions, common diffracted waves are stacked at a point (Figure 2(b)).

The following equation is the travel time equation of diffraction in a cross-well geometry, assuming straight raypaths;

$$t_{ij} = (\sqrt{(VT(0) - S_i)^2 + B^2} + \sqrt{(VT(0) - R_j)^2 + (L - B)^2}) / V \tag{2}$$

where i and j denotes the numbers of the source and of receiver, respectively. $T(0)$ is one way normal time, V is velocity and the other parameters are as shown in Figure 1(b).

The typical procedure of this method is as follows;

step 1 : Set a velocity analysis location and the standard depth (time=0) for the one way normal time $T(0)$.

step 2 : Assume a pair of values for V and $T(0)$ in equation (2) and calculate the travel times for all the pairs of i and j based on equation (2).

step 3 : Obtain the depth by the product of V and $T(0)$ and at this depth point add the amplitudes corresponding to the travel time obtained from step 2. This calculation can be performed by the following equation;

$$\sum_{i=1}^{N_s} \sum_{j=1}^{N_r} A_{T_r}(i, j, t_{ij}) \tag{3}$$

where $A_{T_r}(i, j, t_{ij})$ means the amplitude corresponding to the travel time t_{ij} and N_s and N_r are the total number of source points and receiver points, respectively.

This value gives the concentration of diffraction energy.

step 4 : Repeat steps 1 to 3.

This procedure gives a velocity analysis panel at the location. This panel is a table of numbers as a function of velocity versus one-way normal time. Velocity-time pairs are selected from this panel based on maximum coherency peaks. A series of values along these velocity-time pairs makes a diffraction stacked trace.

3. NUMERICAL EXPERIMENTS

This section describes numerical simulation examples used to demonstrate how the methods work, especially for noisy or complicated data.

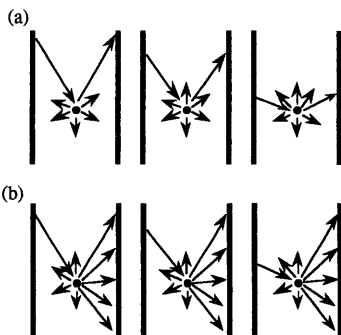


Fig. 2 Comparison of stacked waves between (a) common reflection point and (b) common diffraction point.

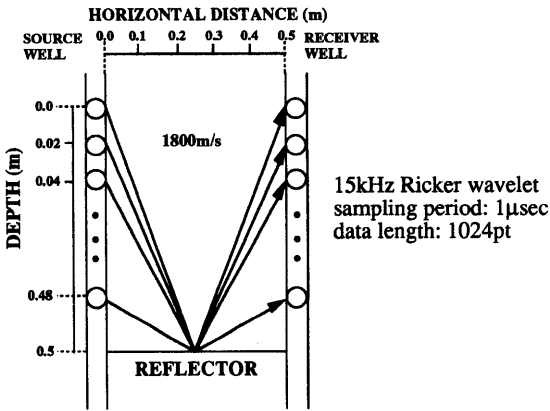


Fig. 3 Numerical simulation model and the specifications of data acquisition. A CDP ensemble with a common depth point at the center of the interwell was produced by using the convolution method.

3.1 CDP STACKING WITH VELOCITY ANALYSIS

Figure 3 shows a numerical simulation model and the specifications of data acquisition. A CDP ensemble with a common depth point at the center of the interwell was used for simplicity. Reflections were generated for a cross-well geometry from the model shown in Figure 3, using the convolution method. Figure 4(a) shows a CDP ensemble. The data processing as described in section 2.1 was performed for this data set. Figure 5(a) shows the result of velocity analysis for the data set shown in Figure 4(a). The concentration of the stacked reflections can be identified clearly.

Next, five Ricker wavelets which have the same frequency and amplitude as those of the reflection were added randomly to each trace of the gather shown in Figure 4(a) (Figure 4(b)). Finally, forty Ricker wavelets were added randomly to each trace of the gather shown in Figure 4(a) (Figure 4(c)). Here, it is assumed that the situation is as after AGC and bandpass filtering. Velocity analysis was performed for each data set. The results are shown in Figure 5(b) and Figure 5(c), respectively. According to the results of the velocity analysis, a CDP stacked record was obtained for each data set (Figure 6(a)–(c)). Figure 6 shows the effectiveness and robustness of the methods for noisy data.

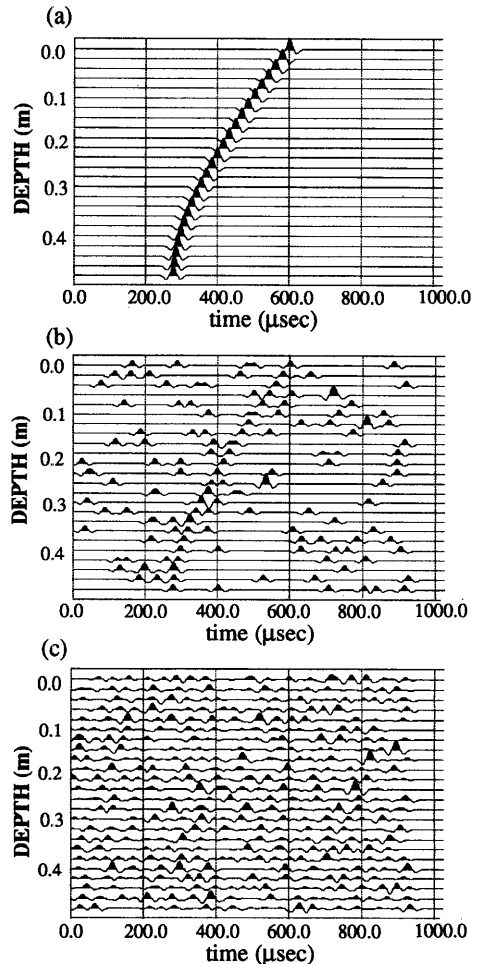


Fig. 4 A CDP ensemble (a) no random noise (b) five random noises are added to each trace (c) forty random noises are added to each trace. Reflected wavefields and random noise were generated by using the convolution method.

3.2 DIFFRACTION STACKING WITH VELOCITY ANALYSIS

Figure 7 shows a numerical simulation model and the specifications of data acquisition. In order to represent scatterers, low velocity points of 3200 m/s are set randomly in a diagonal portion of the background model, which has a uniform velocity 3600 m/s. Numerical simulation data were generated for a cross-well geometry in the model shown in Figure 7 using the finite difference method. Three data sets having vari-

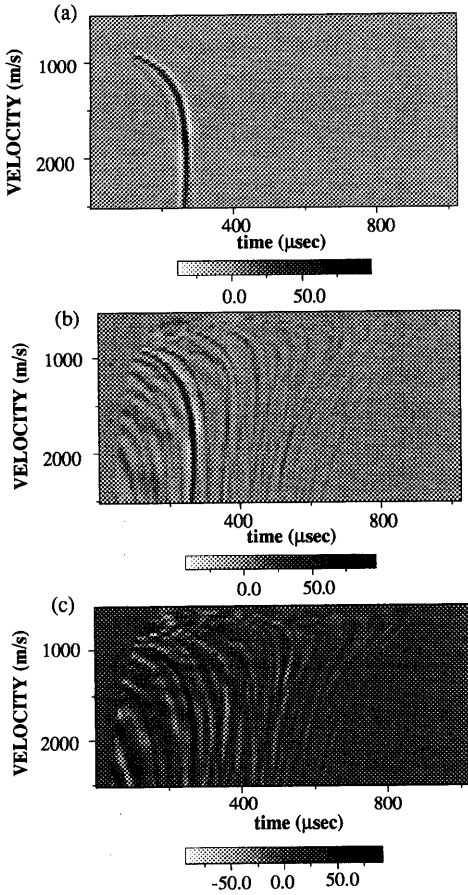


Fig. 5 Results of velocity analysis for each data set shown in Figure 4. The concentration of the stacked reflections can be identified clearly.

ous central frequencies (50 Hz, 100 Hz, 200 Hz Ricker wavelet) were generated. Figure 8 shows examples of common source gathers for each type (after AGC and median filtering). Direct waves were removed by application of median filtering thirty common source gathers were generated for each data set. Data processing as described in section 2.2 was performed on each data set after AGC and median filtering. The positions of velocity analysis are shown in Figure 7. According to the results of the velocity analysis, diffraction stacked records were obtained for each data set (Figure 9). These results lead to the following discussion.

If a shorter wavelength compared to the size of inhomogeneity is used for imaging, high resolu-

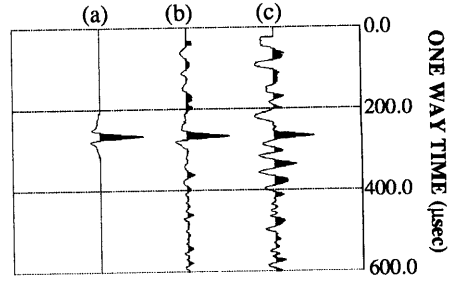


Fig. 6 Results of CDP stacked records for each data set shown in Figure 4.

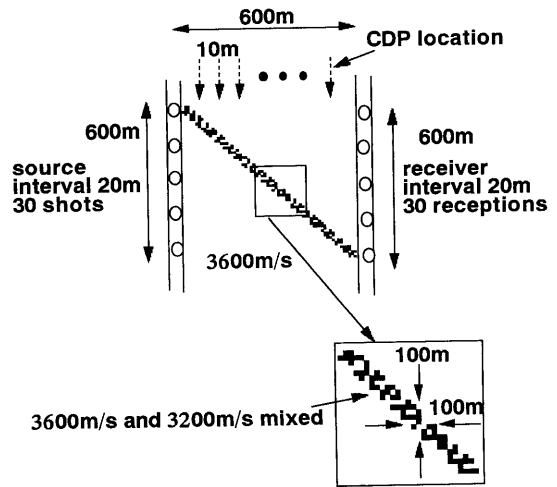


Fig. 7 Numerical simulation model and the specifications of the data acquisition. In order to represent scatterers, low velocity points of 3200 m/s are set randomly in a diagonal portion of the background model, which has a uniform velocity 3600 m/s.

tion stacked records will be obtained but they are noisy. Conversely, if a longer wavelength compared to the inhomogeneity size is used for imaging, low resolution stacked records will be obtained but they are not noisy. The reason for this is the existence of multi-scattering caused by inhomogeneities. Accordingly, in performing data processing in an inhomogeneous region, a suitable wavelength for adequate imaging should be selected.

4. APPLICATION TO FIELD DATA

The methods described in section 2 were applied to field data observed in a geothermal area.

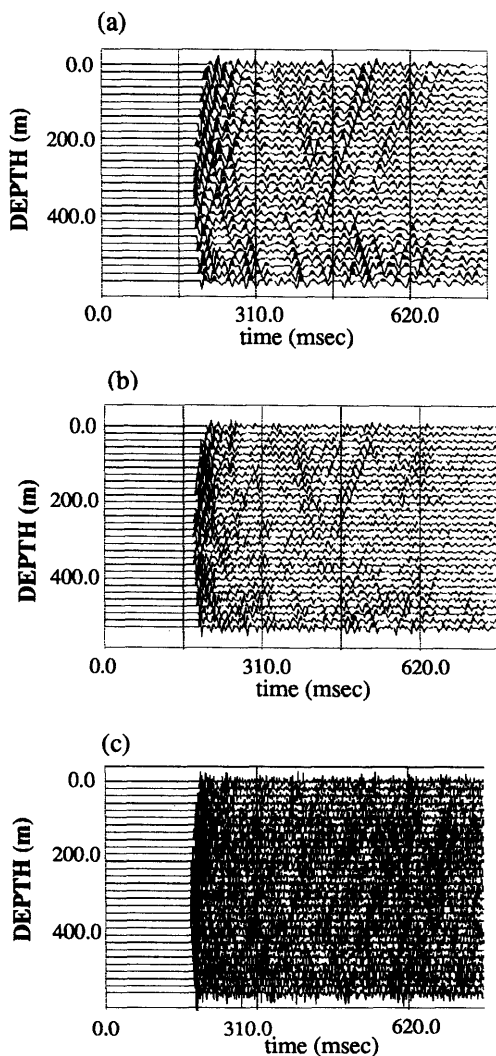


Fig. 8 Examples of common source gather (source depth is 360 m, after AGC and median filtering), central frequency of Ricker wavelet (a) 50 Hz, (b) 100 Hz, (c) 200 Hz. Numerical simulation data were generated by using the finite difference method.

A seismic tomography experiment was carried out by NEDO (New Energy and Industrial Technology Development Organization) in Yutsubo, Oita Pref., Japan using two drillholes, N2-YT-1 and N3-YT-2. Table 1 shows the specifications of the tomographic data acquisition. In this paper, only the vertical component of the data was used for data processing. Figure 10

shows an example of unprocessed common receiver gathers. In Figure 10, the direct P-wave and direct S-wave indicated by the circle were used for spectrum analysis. Figure 11 shows amplitude spectra for both the direct P-wave and the direct S-wave. The frequency of the direct S-wave is lower than that of the P-wave. The P-wave was used for imaging, i.e., velocity analysis was performed almost within the range of P-wave velocity obtained from the P-wave travel-time tomography.

4.1 CDP STACKING WITH VELOCITY ANALYSIS

Figure 12(a) shows the flow chart for this type of data processing. In this case, three ranges of bandpass filtering (180–280 Hz, 80–180 Hz, 30–130 Hz) were applied. The data processing as described in section 2.1 was performed only for the upgoing wavefield. The velocity analysis was performed from 55 m to 215 m at every 2 m interval measuring the distance from the position of N3-YT-2. The standard depth (time=0) for one way normal time was 400 m. Figure 13 shows the CDP stacked records for each frequency range. The calculation CPU time for a sequence of data processing for each frequency range, using the CRAY C90 super computer, was about 3 hours.

4.2 DIFFRACTION STACKING WITH VELOCITY ANALYSIS

Figure 12(b) shows the flow chart for this type of data processing. The data processing as described in section 2.2 was performed after bandpass filtering and AGC. In this case, three ranges of bandpass filtering (180–280 Hz, 80–180 Hz, 30–130 Hz) were applied. The positions of velocity analysis were from 7 m to 263 m at every 2 m interval measuring the distance from N3-YT-2. The standard depth (time=0) for the one way normal time was 400 m. Figure 14 shows the diffraction stacked records for each frequency range. The calculation CPU time for a sequence of data processing for each frequency range, using the CRAY C90, was about 30 hours.

4.3 ESTIMATION OF THE INFLUENCE OF TRANSMITTED P-WAVES IN THE CASE OF THE DIFFRACTION STACKING

In this section, the influence of transmitted

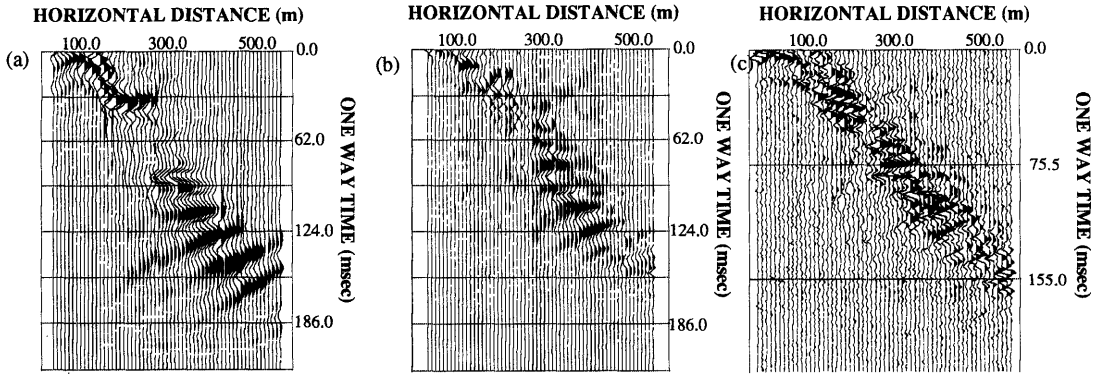


Fig. 9 Results of diffraction stacked record for three types of data set, central frequency of Ricker wavelet (a) 50 Hz, (b) 100 Hz, (c) 200 Hz.

Table 1 Specifications of data acquisition

SOURCE WELL
 SOURCE: PRIMER AND AIRGUN
 INTERVAL: 20m
 SHOT DEPTH: 700-1660m

RECEIVER WELL
 RECEIVER: DS-2 3-COMPONENT RECEIVER
 INTERVAL: 20m
 RECEPTION DEPTH: 660-1670m

RECORD
 RECORD LENGTH: 1.5sec
 SAMPLING PERIOD: 0.25msec

WELL
 PRIMER SOURCE WELL: N2-YT-1
 RECEIVER WELL: N3-YT-2
 AIRGUN SOURCE WELL: N3-YT-2
 RECEIVER WELL: N2-YT-1
 DISTANCE BETWEEN WELLS: 271m

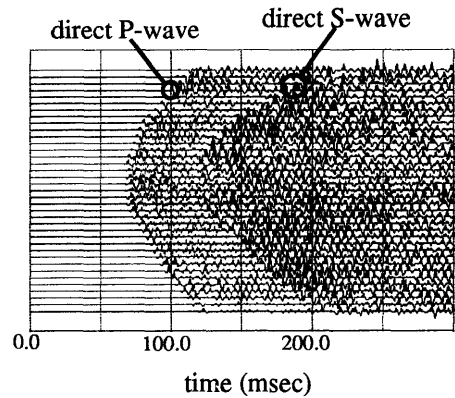


Fig. 10 An example of unprocessed field data. Common receiver gather (receiver depth is 1001.4 m). The direct P-wave and direct S-wave indicated by the circle were used for spectrum analysis.

P-waves in the case of diffraction stacking is estimated. As described in section 4.2, transmitted P-waves were not removed in processing the field data. So, it is necessary to estimate the influence of transmitted P-waves.

4.3.1 MUTE OF TRANSMITTED P-WAVES

Firstly, as a simple method, fifty points were muted from the first arrival picking. Figure 15 shows diffraction stacked records using the muted field data in the case of applying the 80-180 Hz bandpass filtering. There is very little difference between Figure 14(b) (before mute) and Figure 15 (after mute).

4.3.2 RESTRICTION OF THE RANGE FOR STACKED WAVES

As a second method, the range of stacked

waves was restricted in the diffraction stacking. Figure 16 shows the range of stacking. In Figure 16, considering one raypath from one source and assuming a straight raypath, diffractions going through the shadow zone were not stacked. Figure 17 shows the results of the diffraction stacking for various values of θ . Again, the field data processed by application of bandpass filtering (80-180 Hz) was used for imaging. Figure 17 indicates that diffraction stacked records do not fade away with increasing θ .

In the same way, this type of data processing was applied to numerical simulation data. Figure 18 shows a numerical simulation model and the specifications of data acquisition, which were similar to those of the field data acquisition. Nu-

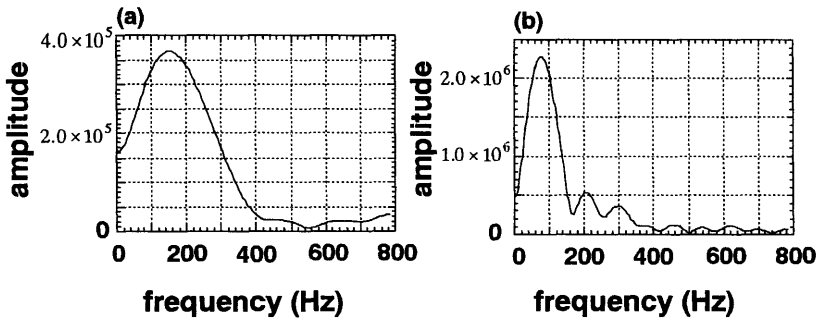


Fig. 11 Comparison of amplitude spectrum between (a) direct P-wave and (b) direct S-wave.

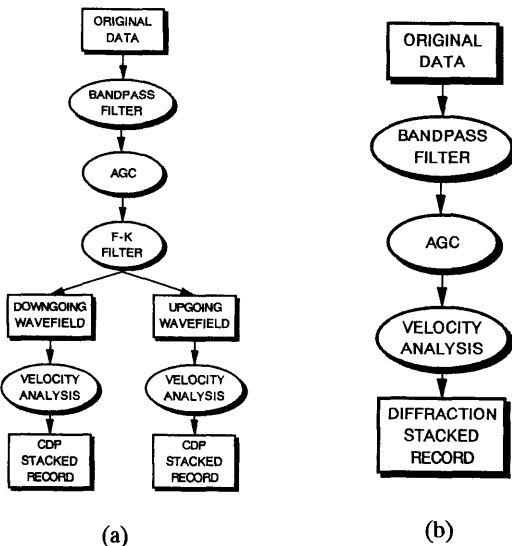


Fig. 12 Flow charts of the data processing for (a) the CDP stacking and (b) the diffraction stacking.

merical simulation data for both transmitted waves and reflections was generated from the model shown in Figure 18 using the convolution method. Thirty common source gathers were generated, and Figure 19 shows an example. Velocity analysis with restriction of the stacked waves was performed at the center of the interwell. Figure 20 shows results of the velocity analysis panel in the case of the diffraction stacking for various values of θ . Figure 20 indicates that the concentration of the transmitted wave does not form a given wavelet (Ricker wavelet). Furthermore, Figure 20 indicates that the concentration of transmitted waves fades away with increasing θ . On the other hand, Figure 17 indicates that

diffraction stacked records do not fade away with increasing θ . Therefore, it can be concluded that diffraction stacked records as shown in Figure 14 are not greatly influenced by transmitted P-waves.

5. DISCUSSION

The results of applying the two types of data processing to the field data leads to the following discussion.

By application of the CDP stacking, adequate stacked records were not obtained. In contrast, the application of the diffraction stacking produced improved stacked records. Some reflectors were delineated. There may not be any marked discontinuity which is intense enough to be imaged. Certainly, geological information (NE-DO, 1992) does not show any large scale fractures or large scale faults in this area. In addition, a result of the P-wave traveltime tomography (YOKOTA *et al.*, 1995) suggests that geological structure in this area consists of nearly horizontal layering. There are two possible reasons for the improved stacked records by the diffraction stacking.

One is the roughness of reflectors. Figure 21 illustrates the influence of reflector roughness on both reflection and diffraction. Of course, the roughness should be compared to the wavelength. If a reflector is rough, reflections are weakened and diffractions are strengthened. In this case, a reflector may be delineated more appropriately by the diffraction stacking than the CDP stacking.

The second explanation is that the diffraction stacking has the potential also for imaging flat reflectors. This hypothesis was tested using some simple numerical experiments. Numerical simula-

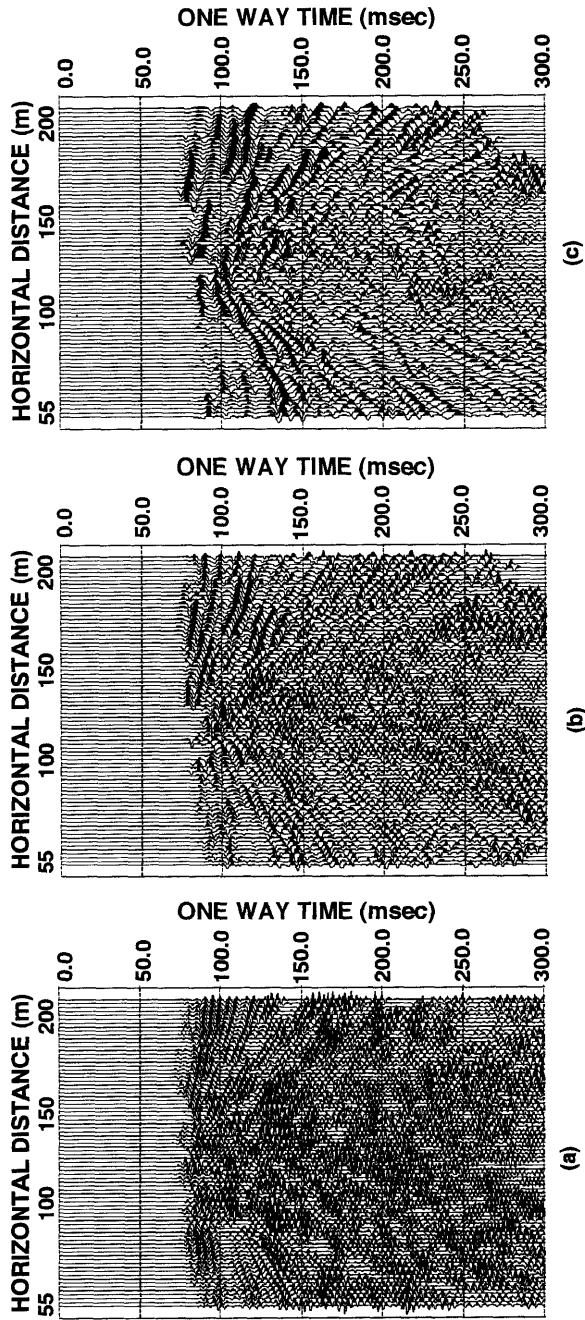


Fig. 13 CDP stacked records for the upgoing wavefield, bandpass filters (a) 180-280 Hz, (b) 80-180 Hz, (c) 30-130 Hz.

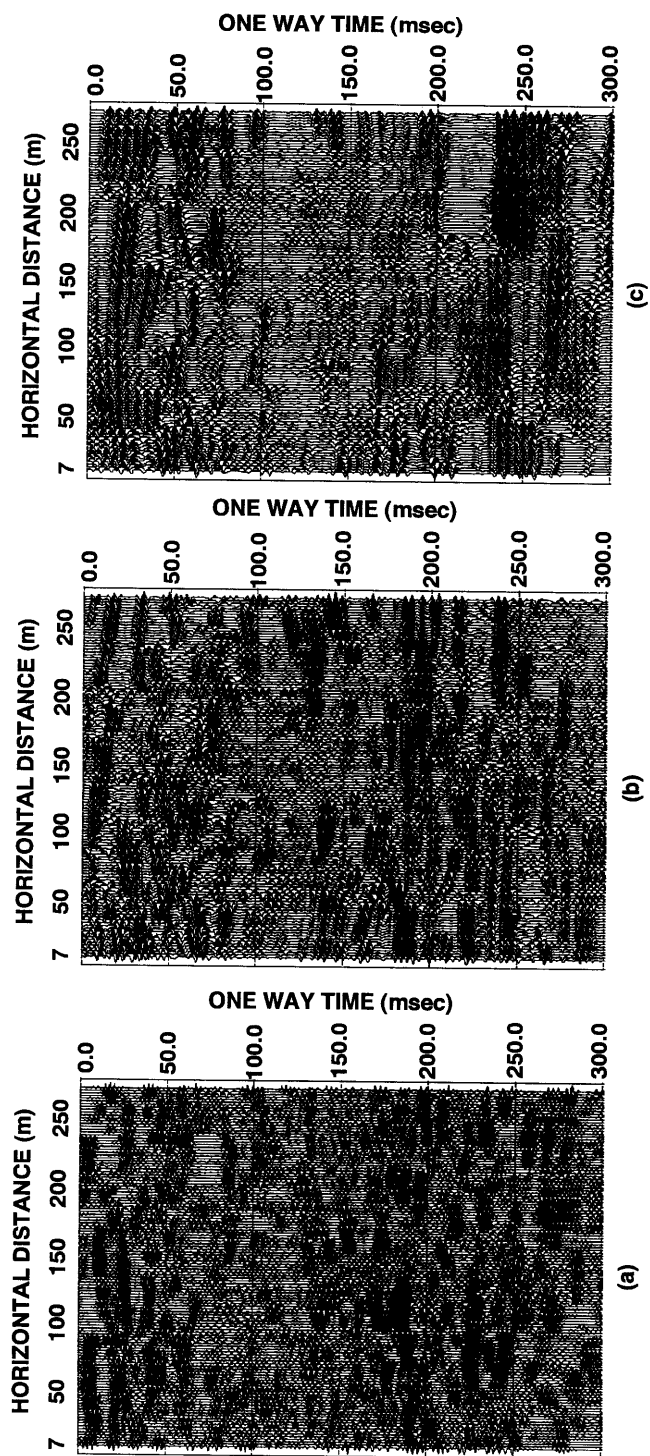


Fig. 14 Diffraction stacked records, bandpass filters (a) 180–280 Hz, (b) 80–180 Hz, (c) 30–130 Hz.

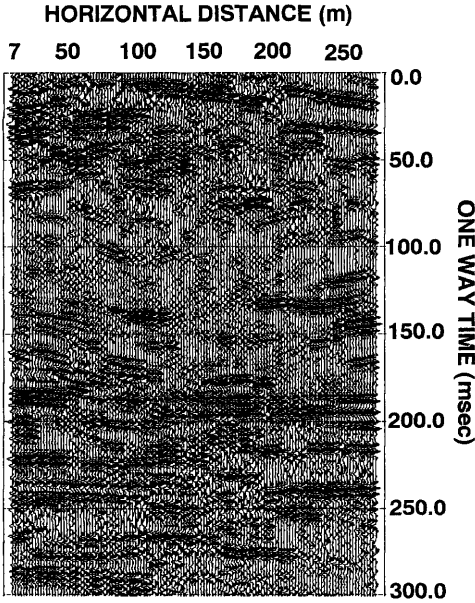


Fig. 15 Diffraction stacked records for the use of the muted field data in the case of applying a bandpass filter (80–180 Hz).

tion model and data acquisition were the same as shown in Figure 18. However, various central frequencies of Ricker wavelet (10 Hz, 50 Hz, 100 Hz, 200 Hz, 400 Hz) were used for obtaining both CDP stacked records and diffraction stacked records. Numerical simulation data for reflections was generated from the model shown in Figure 18 using the convolution method. Thirty common source gathers were generated. Note that the generated data does not have transmitted waves. Both the CDP stacking and the diffraction stacking with velocity analysis were performed for each data set. Figure 22 shows both resulting CDP stacked records and diffraction stacked records at the center of the interwell. Figure 22 indicates that the potential of the diffraction stacking for imaging flat reflectors depends upon the wavelength, while the CDP stacking is not so wavelength dependent. The shorter wavelength is used in the diffraction stacking, the smaller amplitude of the diffraction stacked record is obtained. However, the stack number of the CDP stacking is 30 at the most, while the stack number of the diffraction stacking is invariably 900. Thus S/N of the diffraction stacked record is higher than that of the CDP stacked record. So, the diffraction stacking is effective for obtaining im-

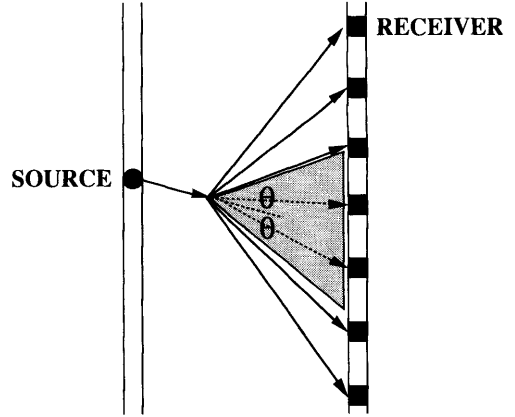


Fig. 16 Diagram illustrating the range of restriction in diffraction stacking. θ is the range of the shadow zone. The diffractions going through the shadow zone are not stacked.

proved stacked records in the case of noisy data. In this respect, more research needs to be done in connection with the shape of reflectors and various types of noise.

Figure 14 indicates that either frequency range of diffraction stacked records is higher than those of corresponding filtered data, because diffraction stacked records were transformed into one way normal time on the time axis. Note that this does not mean that diffraction stacked records transformed into one way normal time have higher resolution than those into two way normal time. This can be explained by Figure 23. Equation (2), which represents the travel time equation in the case of one way normal time, is partially differentiated with respect to $T(0)$. Graphically, the partial differentiation coefficient gives a curved surface, as shown in Figure 23(a). Here, i and j are constant, $S_i=R_j=200\text{ m}$, $L=271.0\text{ m}$ and $B=135.5\text{ m}$. Figure 23(a) indicates the relationship,

$$\frac{\partial t_{ij}}{\partial T(0)} = 2$$

except the part of a trough. This relationship shows that the frequency of the diffraction stacked record is two times as much as the frequency of the data before the diffraction stacking. There is a trough whose peak corresponds to the depth 200 m, the depth of the source and receiver. In the part of a trough, the diffraction record is

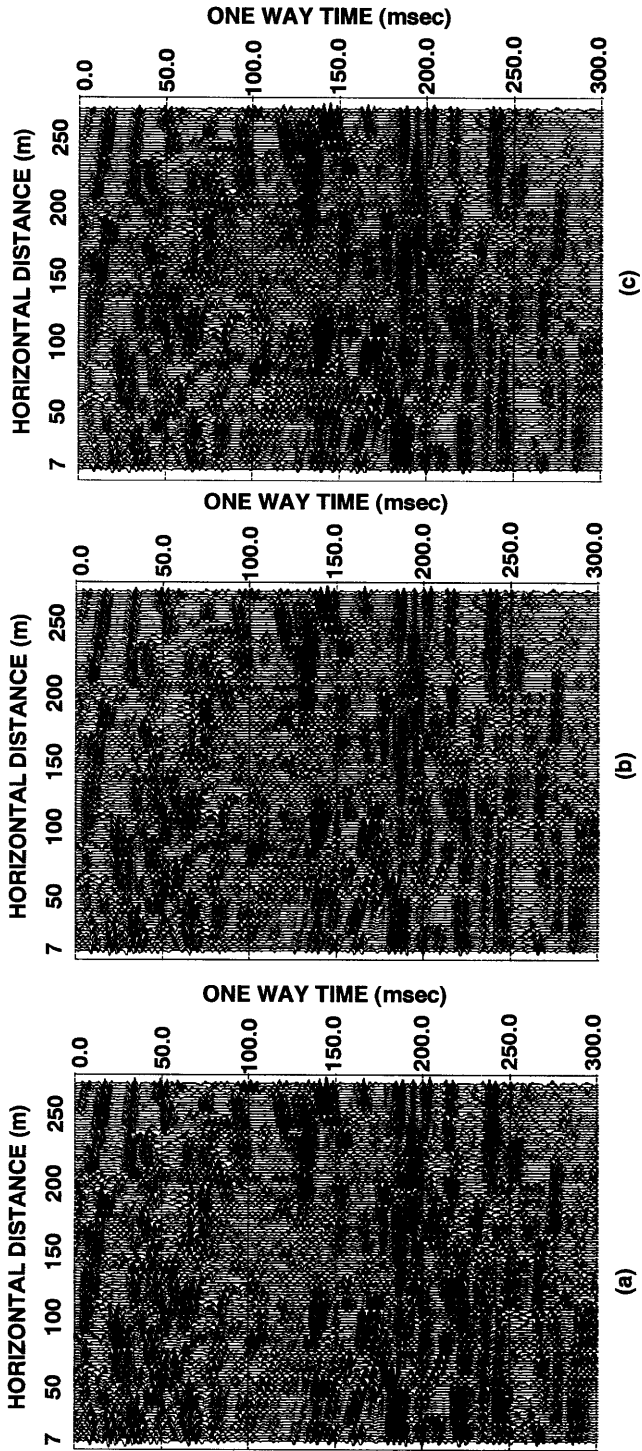


Fig. 17 Diffraction stacked records for various shadow angles θ , (a) $\theta = 0.0$ degree, (b) $\theta = 41.5$ degree, (c) $\theta = 85.2$ degree.

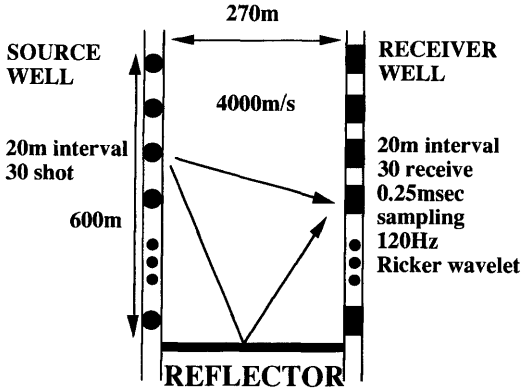


Fig. 18 Numerical simulation model and the specifications of the data acquisition.

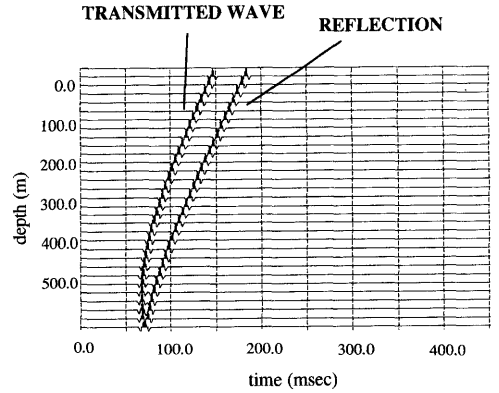


Fig. 19 An example of numerical simulation data. Common source gather (source depth is 0.0 m). Reflections and transmitted waves were generated by using the convolution method.

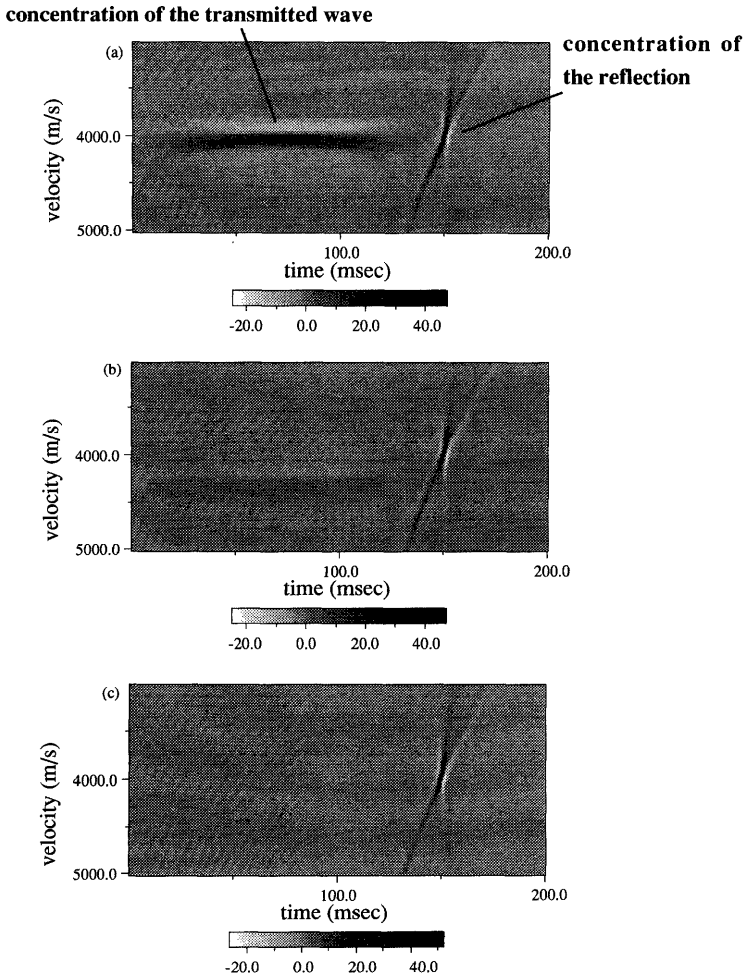


Fig. 20 Results of velocity analysis in the case of diffraction stacking for various shadow angles θ , (a) $\theta = 0.0$ degree, (b) $\theta = 41.5$ degree, (c) $\theta = 85.2$ degree.

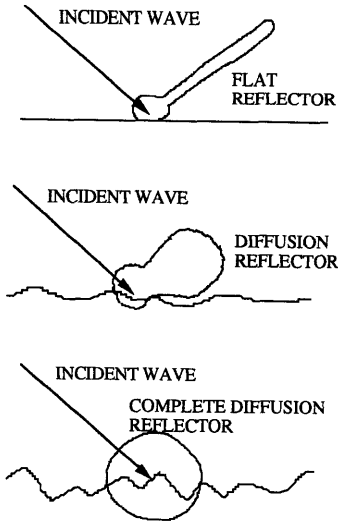


Fig. 21 Diagram illustrating the influence of roughness of reflector on both phenomena of reflection and diffraction.

stretched. Successful imaging cannot be achieved in this region. So it is necessary to eliminate wide angle diffractions in the diffraction stacking.

On the other hand, the travel time equation in the case of two way normal time is represented as follows.

$$t_{ij} = \frac{(\sqrt{(VT(0)/2 - S_i)^2 + B^2} + \sqrt{(VT(0)/2 - R_j)^2 + (L - B)^2}) / V}{(4)}$$

where i and j denotes the number of source and receiver, respectively. T(0) is two way normal time, V is velocity and the other parameters are as shown in Figure 1. Equation (4) is partially differentiated with respect to T(0). Graphically the partial differentiation coefficient gives a curved surface, as shown in Figure 23(b). Here, i and j are constant, $S_i = R_j = 200\text{ m}$, $L = 271.0\text{ m}$ and $B = 135.5\text{ m}$. Figure 23(b) indicates the following relationship,

$$\frac{\partial t_{ij}}{\partial T(0)} = 1$$

except the part of a trough. This indicates that the frequency of the diffraction stacked record corresponds to the frequency of the data before the diffraction stacking. Again, there is the same kind of trough whose peak corresponds to the depth 200 m, the depth of the source and

receiver.

It follows from the above that the rate of change of travel time for one way normal time is two times as much as that of two way normal time.

6. CONCLUDING REMARKS

In this paper, two types of data processing are presented, together with numerical simulation examples in order to evaluate these methods for noisy or complicated data. Finally, a preliminary application of the methods to field data observed in a geothermal area is described. The proposed data processing methods, especially the diffraction stacking, has the potential for rough imaging as a first step before more precise imaging is performed, especially in geothermal or other inhomogeneous areas.

Certainly, cross-well seismic methods have the potential for higher resolution imaging than surface seismic methods. However, especially in the inhomogeneous area, the use of the high frequency waves may cause problems in delineating detailed geological structure of discontinuities (fractures of faults). In this respect, further research needs to be done to determine

1. the most suitable wavelength for adequate imaging;
2. the relation between the roughness of the reflector and the wavelength; and
3. how to select the most suitable traces in the case of the diffraction stacking.

ACKNOWLEDGMENTS

The authors would like to thank the New Energy and Industrial Technology Development Organization for permission to use the data.

References

HARRIS, J. M., RECTOR, J. W., LAZARATOS, S. K., and VAN SCHAACK, M. (1992) : High resolution cross-well imaging of a west Texas carbonate reservoir : *part 1, presented at the 62nd Ann. Internal. Mtg. of SEG, expanded abstracts*, 35-39.

ISHII, Y., MURAOKA, H., ASAKURA, N., ONISHI, M. (1995) : Cross-well seismic tomography for geothermal exploration, *Proceedings of the 3rd SEG/SEG International Symposium on Geotomography*, 368-374.

LAZARATOS, S. K., RECTOR, J. W., HARRIS, J. M., and VAN SCHAACK, M. (1993) : High-resolution, cross-well, reflection imaging : Potential and technical

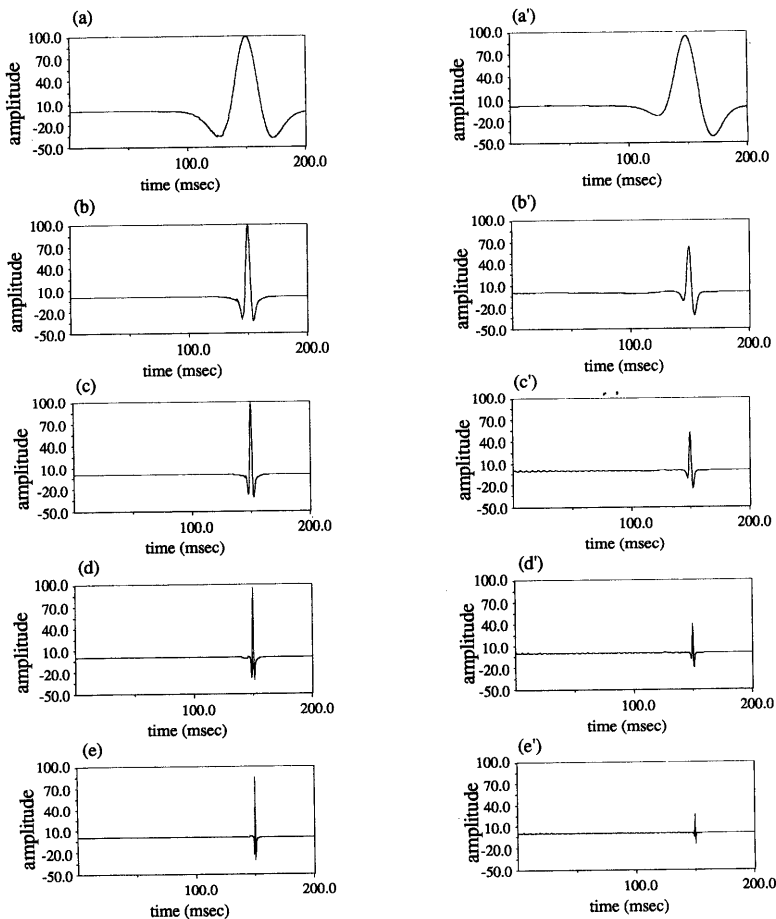


Fig. 22 Both results of CDP stacked records and diffraction stacked records at the center of the interwell, for various central frequencies of Ricker wavelet, (a) 10 Hz, (b) 50 Hz, (c) 100 Hz, (d) 200 Hz, (e) 400 Hz. The symbol ' means the results of the diffraction stacking.

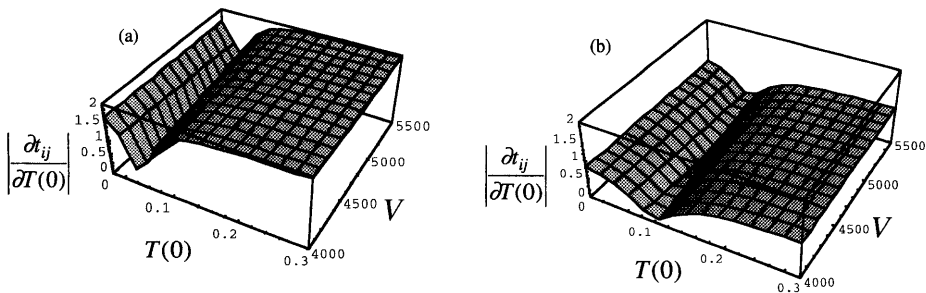


Fig. 23 3-D plot of the partial differentiation coefficient $|\partial t_{ij}/\partial T(0)|$ (a) in the case of one way normal time, (b) in the case of two way normal time.

- difficulties, *Geophysics*, **58**, 1270-1280.
- MATSUSHIMA, J., ROKUGAWA, S., YOKOTA, T., MIYAZAKI, T. (1995a) : Application of CDP stacking to cross-well data —Imaging with cross-well diffraction data—, *Proc. of 92th SEGJ Conf.*, 37-41, (In Japanese with English abstract).
- MATSUSHIMA, J., ROKUGAWA, S., YOKOTA, T., MIYAZAKI, T. (1995b) : Application of CDP stacking to cross-well data —Application to the field data—, *Proc. of 93rd SEGJ Conf.*, 236-240.
- New Energy and Industrial Technology Development Organization (1992) : *Confirmation study of the effectiveness of prospecting techniques for deep geothermal resources, Development of seismic exploration techniques, Development exploration techniques for fracture-type reservoir, Drilling, well logging, well test and integrated assessment of fracture characteristics (Abstract) (22p)*, (In Japanese with English abstract).
- ROKUGAWA, S. and MATSUSHIMA, J. (1995) : Application of CDP stacking to cross-well reflection data —Consideration by Numerical Simulation and Experimental Scale Model—, *BUTSURI-TANSA*, **48**, 85-98, (In Japanese with English abstract).
- ROBERT, R. S. (1990) : Crosswell Seismic Imaging Using Reflections, *Geotomography* vol. 1, *Proceedings of the 1st SEGJ/SEG International Symposium on Geotomography*, 45-53.
- SAM G. and LARRY L. (1992) : Cross-borehole tomographic migration, *Journal of seismic exploration*, **1**, 315-324.
- VAN SCHAACK, M., HARRIS, J. M., RECTOR, J. W. and LAZARATOS, S. K. (1992) : High resolution cross-well imaging of a west Texas carbonate reservoir : part 2, presented at the 62nd Ann. Internat. Mtg. of SEG, expanded abstracts, 40-44.
- YOKOTA, T., ROKUGAWA, S., MATSUSHIMA, J., MIYAZAKI, T. (1995) : Application of S-wave tomography to the geothermal area : A case study at Yutsubo geothermal area, *Proceedings of the 3rd SEGJ/SEG International Symposium on Geotomography*, 375-382.

速度解析をともなう CDP 重合及び散乱重合による坑井間イメージング

松島 潤・六川修一・横田俊之・宮崎光旗

要 旨

地下深部の詳細な構造，特にフラクチャなどの断裂系をイメージングする弾性波利用探査技術は地熱貯留層解明や活断層調査にとって有効な技術となりうる。

複数の坑井を利用した探査は地表からの探査に比べて高分解能であるため，上記の目的を達成しうる技術として期待され，近年盛んに研究が行われている。なかでも初動走時を用いた走時トモグラフィは技術的に確立されてきており，実フィールドへの応用も進んでいる。しかし，波の現象として積分効果を利用するこの走時トモグラフィは，波が本来持っている分解能を生かすことができない欠点がある。

そこで本研究では坑井間の幾何的配置において観測される反射波あるいは散乱波に着目した以下に述べる 2 種類のデータ処理を提案した。反射波及び散乱波はいつれも，波の現象としては微分効果を反映しているため，これらの波を利用したイメージングは，波が本来持っている分解能を生かすことかできる。

- (1) 従来型の地表反射法の中核技術である速度解析及び CDP 重合を坑井間の幾何的配置において適用した。
- (2) CDP 重合法の概念を以下に述べるように拡張することにより，散乱波を対象としたイメージングを考えた。

『地層は散乱体の集合であると仮定し（すべての点で入射波は散乱波を発生すると仮定），ある点で共通散乱する波を選び出しそれらを重合する。』

上記 2 種類のデータ処理を数値実験データに適用し，S/N の悪いデータあるいは複雑な波動場に対して，筆者等の提案する手法が有効であることを示した。さらに地熱フィールドにおいて実際に取得されたデータに対して本手法を予備的に適用した。その結果，散乱波を重合するデータ処理によって良好と思われる結果を得た。この理由に関して数値実験等をまじえて議論した。